CHAPTER VI
PREPARATION AND CHARACTERIZATION OF HEXANOYL CHITOSAN/POLYLACTIDE BLEND FILMS

6.1 ABSTRACT

In the present contribution, blend films of hexanoyl chitosan (H-chitosan) and polylactide (PLA) were prepared by the solution-casting technique from the corresponding blend solutions in chloroform. Fourier-transformed infrared spectroscopy results indicated no significant interaction between H-chitosan and PLA molecules. The thermal degradation behavior of the as-prepared blend films was found to be intermediate to those of the pure components. Only the blend film having the H-chitosan content of 20 wt.% exhibited the degradation temperature greater than those of the pure components. All of the blend films exhibited one composition-dependent glass transition temperature, indicating partial miscibility between H-chitosan and PLA molecules in the bulk amorphous phase. The apparent degree of crystallinity of the PLA component in the blends was found to decrease monotonically with increasing H-chitosan content. Both the tensile strength at break and the Young's modulus of the blend films were found to decrease from that of the pure PLA to that of the pure H-chitosan with increasing H-chitosan content.

(**Key-words**: chitosan; hexanoyl chitosan; polylactide; polymer blend)

6.2 INTRODUCTION

Polymer blending is an attractive alternative for producing new polymeric materials with tailored properties without having to synthesize totally new materials. Other advantages for polymer blending are versatility, simplicity, and inexpensiveness.

Nowadays, natural polymeric materials have become increasingly important due to their natural abundance and low costs. Chitin is one of the most abundant polysaccharides and can be found in various invertebrates and lower plants. Chitosan is one of chitin's derivatives, achieved by N-deacetylation of chitin, even though the reaction is never complete [1]. There is not yet a formal nomenclature for describing chitosan of various degrees of deacetylation. Chitosan is known to be non-toxic, odorless, biocompatible with living tissues, biodegradable, and chemically functionalizable. Due to these advantages, chitosan and its derivatives are seen in applications such as biomedical materials, biodegradable packaging, cosmetics, metal ion-capturing materials for waste-water treatment, and so on so forth [2].

Due to the abundance of hydrophilic functional groups, chitosan is not soluble in most organic solvents. In order to solve this problem, some chemical modifications to introduce hydrophobic nature to chitosan such as phthaloylation [3], alkylation [4], and acylation [5-7] reactions can be done. Organically soluble derivatives of chitosan can be used to formulate by-designed materials for biomedical applications such as polymeric drugs and artificial organs with high specificity and wide applicability. Acylated chitosans are soluble in various organic solvents, such as chloroform, benzene, pyridine, and tetrahydrofuran (THF). *N*-acylchitosan has been fabricated as membranes [8], fibers [9], and films [10]. *N*-hexanoyl chitosan was found to exhibit the best blood compatibility in comparison with *N*-propionyl, *N*-butyryl, and *N*-pentanoyl chitosans [11]. Furthermore, *N*-hexanoyl and *N*-octanoyl chitosans were found to be anti-thrombogenic and resistant to hydrolysis by lysozyme [12]. As a result, acylated chitosans are very interesting derivatives of chitosan to be used in biomedical applications.

Among the various aliphatic degradable polyesters, polylactide (PLA) has been considered as one of the most interesting and promising biodegradable

materials and has been used in medical applications, such as surgical sutures [13], drug delivery systems [14], and bone fixtures [15]. The use of these products in vivo has a tremendous advantage over traditional products due to the fact that PLA can be metabolized directly inside the body [16]. The increasing use of biodegradable polymers in medicine has attracted polymer scientists and the likes in pursuit of new materials that exhibit unique properties for specific applicability in the field.

In the present contribution, blend films of hexanoyl chitosan (H-chitosan) and PLA were prepared by the solution-casting technique. Chloroform was used as the solvent. The effect of blend composition on miscibility, morphology, thermal properties, and mechanical properties was investigated. The main objective of this work was to find an economical way for improving the applicability of H-chitosan through the blending with PLA.

6.3 EXPERIMENTAL

Materials

Chitosan having the degree of deacetylation of ca. 91% was prepared from shrimp shells by acid and alkali treatments. Chitosan was pulverized into powder, the size of which ranged from 71 to 75 μm, prior to further use. Other chemicals used were hexanoyl chloride (Fluka, Switzerland), methanol [Labscan (Asia), Thailand], pyridine (Sigma-Aldrich, USA), and chloroform (Sigma-Aldrich, USA). Both pyridine and chloroform were distilled and later dried via molecular sieve prior to use. The other chemicals were analytical grade and were used as-received. PLA was supplied as courtesy from Daiseru Chemicals (Japan). The viscosity-average molecular weight $\overline{M}_v$ of PLA was determined, based on viscosity measurements at 25°C in chloroform following the Mark-Houwink equation of the form [17]: $[\eta] = 7.4 \times 10\text{-}5 \cdot \overline{M}_v\, 0.87$, to be ca. 70,000 g·mol^{-1}.

Synthesis and Characterization of H-chitosan

H-chitosan was synthesized by reacting chitosan with hexanoyl chloride in a mixture of anhydrous pyridine and chloroform, as shown in Figure 6.1. The hexanoylation of chitosan was thoroughly described in an earlier work by Zong *et al.* [7]. Normally, the hexanoylation reaction is never complete. In this work, the hexanoylation reaction of chitosan was repeated for four times in order to obtain the highest possible degree of substitution of the resulting H-chitosan (viz. the maximum degree of substitution is 4.00, see Figure 6.1). To confirm the chemical structure and the degree of substitution, the obtained H-chitosan was characterized by Fourier-transformed infrared spectroscopy (FT-IR) and elemental analysis (EA) techniques.

Preparation of Blend Films

To prepare blend films of H-chitosan and PLA, solutions of H-chitosan and PLA were first separately prepared at the concentration of 1% w/w in chloroform. Slight stirring was used to expedite the dissolution and to homogenize the solutions. Blend films of different compositions (i.e. the weight ratios between H-chitosan and PLA of 100/0, 80/20, 60/40, 50/50, 40/60, 20/80, and 0/100, respectively) were then prepared by casting a mixture of the solutions in a respective weight ratio on a Teflon dish. It should be noted that slight stirring was used to homogenize the mixture prior to pouring onto the dish. The casting was let dry at room temperature for one day and later at room temperature in vacuo for another two days.

Characterization Techniques

FT-IR spectroscopy was used to characterize chemical functional groups of as-synthesized H-chitosan and as-prepared blend films. FT-IR spectra were collected on a Bruker Instrument Equinox55 FT-IR spectrometer at a resolution of 4 cm^{-1}. Elemental analysis was used to determine the degree of substitution of the hexanoyl groups on chitosan chains. The measurement was carried out on a Perkin Elmer PE2400 Series II CHNS/O analyzer at the combustion temperature of 950°C. Samples of approximately 1 to 2 mg were filled in tin foil and analyzed in air using oxygen as a combustion gas (under a flow rate of 20 $ml \cdot min^{-1}$) and helium as a carrier gas (under a flow rate of 200 $ml \cdot min^{-1}$). Thermal properties of the blend films

were analyzed by differential scanning calorimetry (DSC) and thermogravimetric analysis (TGA). DSC thermograms were recorded on a Mettler DSC 822e/400 analyzer at a heating rate of 10°C·min^{-1} under nitrogen atmosphere. Samples of around 5 to 10 mg were used for the DSC measurements. TGA patterns were measured on a Perkin Elmer Pyris Diamond TG/DTA analyzer at a heating rate of 10°C·min^{-1} under nitrogen atmosphere over the temperature range of 30 to 750°C. Samples of approximately 10 to 20 mg were used for the TGA measurements. Wide-angle X-ray diffraction (WAXD) was used to observe the crystal structure of the blend films. WAXD patterns were obtained on a Rigaku Rint2000 X-ray diffractometer. The X-ray source was CuKα. The measurements covered the scanning range of 5 to 40° at a scanning speed of 5 deg·sec^{-1}. Phase morphology of the blend films was investigated by a JEOL 520-2AE scanning electron microscope (SEM). Prior to observation under SEM, the blend films were either etched with cyclohexane or concentrated acetic acid solution to remove either H-chitosan or PLA, respectively, for two minutes at room temperature. Finally, a Lloyd LRX universal testing machine was used to assess the mechanical properties of the blend films. A load cell of 500 N was used along with a 500-mm·min^{-1} cross-head speed and a 50-mm gauge length.

6.4 RESULTS AND DISCUSSION

Chemical structure of As-synthesized H-chitosan

The as-synthesized H-chitosan was characterized by FT-IR and EA for its chemical structure and the degree of substitution of the hexanoyl group along chitosan chains. The FT-IR spectrum for the obtained H-chitosan (see the topmost curve with the label of 100/0 in Figure 6.2) exhibited the following characteristic peaks (and the corresponding assignment) at 1716 cm^{-1} [C=O of $N(COR)_2$], 1747 cm^{-1} (C=O of OCOR), 2957 cm^{-1} (νas of CH_2), 2932 cm^{-1} (νas of CH_2), 2872 cm^{-1} (νas of CH_2), 1465 cm^{-1} (νs of CH_2), and 1171 cm^{-1} (twisting vibration of CH_2). That the characteristic absorption band around 3000 to 4000 cm^{-1} for chitosan (assigned to OH and NH_2) was absent from the FT-IR spectrum observed indicates

that hexanoyl groups substituted at the hydroxyl and the amino groups along the chitosan chains. The EA result for the H-chitosan synthesized after four times of the hexanoylation reaction of chitosan revealed the molar percentage of C, H, and N atoms as 66.48, 10.01, and 2.68%, respectively. In comparison with the calculated values of 64.89, 9.17, and 2.56% for H-chitosan of a perfect degree of substitution (see Figue 6.1), the degree of substitution of the hexanoyl group along chitosan chains for the H-chitosan synthesized was 3.92, which is very close to the theoretical value of 4.00. Both FT-IR and EA results confirm a successful synthesis of H-chitosan.

Characterization of H-chitosan/PLA Blend Films

Chemical Characteristics

Blend films of H-chitosan and PLA in various blend compositions were prepared using chloroform as the common solvent. To investigate the chemical characteristics of the obtained films, FT-IR was employed. Figure 6.2 shows FT-IR spectra of films of pure H-chitosan (i.e. the topmost curve), pure PLA (i.e. the bottommost curve), and H-chitosan/PLA blends. It is apparent from Figure 6.2 that the characteristic carbonyl-stretching absorption peak of H-chitosan at 1716 cm^{-1} (C=O of $N(COR)_2$) was present in all of the spectra observed (with an exception of that of the pure PLA), whereas the characteristic carbonyl-stretching absorption peak of PLA at 1768 cm^{-1} (C=O of OCOR) was present in all of the spectra observed (with an exception of that of the pure H-chitosan). The intensity of these peaks was found to be more pronounced with an increase in the content of the respective content. Since, apart from the absorption peaks specific to H-chitosan and PLA being observed in all of the blend films, no additional peaks signifying possible interaction between H-chitosan and PLA were observed, it is logical to postulate that the interaction between H-chitosan and PLA might be either non-existent or too weak to be detected by FT-IR.

Figure 6.3 shows characteristic absorption peaks at 756 and 870 cm^{-1} which have been assigned to the crystalline and the amorphous phase of PLA [18]. Obviously, the intensity of both peaks was found to decrease with decreasing PLA content in the blends. Relatively, the decrease in the intensity of the crystalline peak

was more pronounced than the decrease in the intensity of the amorphous peak. The ratio between the intensity of the crystalline peak to that of the amorphous peak for blend films was found to decrease from that of the pure PLA film and decrease with further increasing H-chitosan content. The crystalline peak was almost unnoticed in the blend film having the H-chitosan content of 80 wt.%. The results suggest that the apparent degree of crystallinity of the PLA phase in the blend films decreased with addition and increasing H-chitosan content.

Thermal Characteristics

Thermal Degradation

Thermal stability of pure H-chitosan, pure PLA, and corresponding blend films was evaluated by TGA technique. Figure 6.4 shows TGA results for pure H-chitosan, pure PLA, and 50/50 w/w H-chitosan/PLA blend films. According to the derivative TGA curves, pure PLA film was found to degrade at ca. 327°C, while pure H-chitosan film exhibited two degradation peaks at ca. 257 and 327°C, respectively. Apparently, the 50/50 H-chitosan/PLA blend film exhibited degradation behavior intermediate to those of the pure components, exhibiting two degradation peaks at ca. 253 and 312°C, respectively. Table 6.1 summarizes the observed degradation peak value(s) (denoted T_d) for all of the films investigated. For most blend films, their degradation behavior was found to be intermediate to those of the pure components. Interestingly, only 20/80 H-chitosan/PLA blend film exhibited only one degradation peak, with the observed Td value being much greater than those of the pure components.

Glass Transition Temperature

One important parameter used to investigate whether two polymers are miscible in the amorphous phase is the glass transition temperature T_g. It is also well known that, for semi-crystalline polymers, T_g is quite difficult to measure. Indeed, the rigid amorphous phase, located between the lamellae and the bulk amorphous phase, does not transform into a mobile, amorphous liquid phase at T_g and is not quite observable by a common DSC in the usual conditions used for the

measurement of this parameter. Since this rigid amorphous interfacial region often accounts to a great extent to the discrepancies in the measurement of the crystalline and the bulk amorphous contents, polymers are usually quenched from the melt to a temperature situated well below T_g to decrease its importance.

In DSC, the miscibility of two polymers in the bulk amorphous phase can be evaluated by the presence of a single, composition-dependent T_g value between those of the constituent polymers. In order to measure the T_g for the blend films prepared, each blend film sample was heated from room temperature to 200°C at a heating rate of $10°C \cdot min^{-1}$. After thermal equilibration, the sample taken out from the DSC furnace, while in the sample holder, and was quenched in liquid nitrogen in order to maximize the bulk amorphous content in the sample. After 20 min of submersion in liquid nitrogen, the sample was put back into the DSC furnace, the temperature of which was equilibrated at room temperature, and a second heating scan was subsequently carried out as soon as the temperature of the sample equilibrated to that of the DSC furnace. The observation of T_g was then carried out on this second heating scan.

No obvious T_g was observed in the DSC thermogram obtained for pure H-chitosan film, while a T_g of around 50°C was observed for pure PLA film (see Table 6.2). The value of 50°C observed for pure PLA film is in general accord with the value of 56°C observed by thermo-mechanical analysis [19]. For all of the blend films investigated, one composition-dependent T_g was clearly observed for each blend composition (see Table 6.2). Interestingly, the observed T_g value was only found to decrease with addition and increasing H-chitosan content when the H-chitosan content was lower or equal to 40 wt.%, while it was found to be unchanged with further increase in the H-chitosan content. At "low" H-chitosan contents (i.e. $\leq$ 40 wt.%), the observed slight decrease in the T_g of the blend products from that of the pure PLA could be a result of the partial miscibility of H-chitosan and PLA molecules in the amorphous phase, but, with further increase in the H-chitosan content, the restricted mobility of PLA molecules due to the presence of H-chitosan molecules could result in the constancy of the resulting T_g values.

Melting Behavior and Apparent Degree of Crystallinity

Prior to observing the melting behavior and the apparent degree of crystallinity, each sample was pre-conditioned in the same manner in order to set the thermal history of the sample by heating each sample from room temperature to 200°C at a heating rate of 10°C·min^{-1} and immediately cooling it down at a cooling rate of 10°C·min^{-1} to room temperature. The thermogram for the second heating scan was recorded for further analysis.

Figure 6.5 shows heating thermograms for pure H-chitosan, pure PLA, and H-chitosan/PLA blend films. Evidently, no thermal transition of any kind was discernable in the heating thermogram for pure H-chitosan. For both pure PLA and corresponding blend films of various compositions, either one or two melting endotherm(s) was observed. Based on related studies on multiple melting behavior of some other semi-crystalline polymers [20,21], the occurrence of the low-temperature melting endotherm was usually attributed to the melting of the primary crystals, while that of the high-temperature melting endotherm was to the melting of the re-crystallized crystals formed during a heating scan.

The peak temperature of the low-temperature melting endotherm denotes T_{ml}, while that of the high-temperature one denotes T_{mh}. These values for all of the samples investigated are summarized in Table 6.2. For pure PLA film, the observed T_{ml} and T_{mh} values were found to locate at 162 and 170°C. The apparent melting peak at 162°C is in good agreement with the reported value of 165°C [19]. With increasing H-chitosan content, both the T_{ml} and the T_{mh} values were found to slightly decrease from that of the pure PLA, and no significant dependency of these values on H-chitosan content was observed.

Another important information which can be deduced from the thermograms shown in Figure 6.4 is the apparent degree of crystallinity that was present in each of the as-cast films. Qualitatively, the area under the melting endotherm related directly to the amount of the crystals present within the film sample. Since it was postulated that the high-temperature melting endotherm related to the melting of the crystals formed during the heating scan, only the low-temperature melting one should be accounted for the amount of the primary crystals present within each sample.

ต้นฉบับ หน้าขาดหาย

micrographs were PLA particles which were dissolved away after the blend films were immersed in concentrated acetic acid solution for two minutes.

From these micrographs, H-chitosan and PLA were found to phase-separated during the evaporation of the solvent. When H-chitosan was the minor phase, the H-chitosan particles were found to distribute quite regularly throughout the PLA matrix and the size of the particles became smaller, while the number of the particles was found to increase, with increasing amount of H-chitosan from 20 to 50 wt.%. On the other hand, when PLA was the minor phase, the PLA particles were found to distribute very regularly throughout the H-chitosan matrix and the size of the particles was found to increase, while the number of the particles was found to decrease, with increasing amount of PLA from 20 to 50 wt.%. Comparatively, PLA minor phase was found to distribute much evenly in the matrix than that of the H-chitosan minor phase.

Crystalline Structure

WAXD patterns for pure H-chitosan, pure PLA, and all of the blend films investigated are illustrated in Figure 6.7. Obviously, the WAXD pattern for pure H-chitosan film exhibited a sharp diffraction peak at the scattering angle 2θ of around 6.0° along with a broad diffraction peak centering at the 2θ of around 18.7°. The sharp diffraction peak at about 6.0° was reported to be a result of the interdegitation of the hexanoyl side-chains with the extended main chains forming a layer structure, while the broad diffraction peak at about 18.7° was a result of the loss of crystallinity due to the loss of hydrogen bonding [7]. For pure PLA film, the obtained WAXD pattern showed only one broad diffraction peak centering at the 2θ of around 16.9°. When crystallizing in a pseudo-orthorhombic unit cell (with axes a = 1.07 nm, b = 0.595 nm, and c = 2.78 nm), PLA should show main diffraction peaks at the 2θ's of 15, 17, and 19° [23]. For H-chitosan/PLA blend films, the obtained diffraction patterns appeared to contain the diffraction peaks characteristic to both pure H-chitosan and pure PLA. No significant shift in the diffraction peaks was observed, suggesting that the presence of one component did not affect the ordered structure which would be observed for the other component.

Tensile Properties

The mechanical properties of the as-cast films were tested in terms of the tensile strength at break, the percentage of elongation at break, and the Young's modulus. All of these results are shown graphically in Figure 6.8. For pure H-chitosan film, the tensile strength at break, the percentage of elongation at break, and the Young's modulus were found to be ca. 1.8 MPa, 890%, and 240 MPa, respectively. On the other hand, pure PLA film was found to be much more brittle, with the tensile strength at break, the percentage of elongation at break, and the Young's modulus being 33.3 MPa, 10%, and 1390 MPa, respectively. For H-chitosan/PLA blend films, both the tensile strength at break and the Young's modulus were found to decrease from that of the pure PLA to that of the pure H-chitosan with an increase in the H-chitosan content. On the contrary, the percentage of elongation at break was found to initially increase with an addition of H-chitosan of about 20 wt.%, gradually decrease with further addition of H-chitosan from 20 to 50 wt.%, and finally increase with further addition of H-chitosan from 50 wt.% to reach that of the pure H-chitosan. Physically, the blend films appeared to be softer and more elastic as H-chitosan content increased. The non-linear dependency of the observed mechanical properties on the blend composition suggests that phase separation should occur in the H-chitosan/PLA blend films.

6.5 CONCLUSIONS

Hexanoyl chitosan (H-chitosan) was successfully synthesized by repeated hexanoylation of chitosan for four times. The as-synthesized H-chitosan had the degree of substitution of the hexanoyl group along the chitosan chains of 3.92. Blend films of H-chitosan and polylactide (PLA) were prepared by the solution-casting technique from corresponding blend solutions in chloroform. Fourier-transformed infrared spectroscopy results indicated that no significant interaction between H-chitosan and PLA molecules was observed. The thermal degradation behavior of the as-prepared blend films was found to be intermediate to those of the pure components. Only the blend film having the H-chitosan content of 20 wt.% exhibited the degradation temperature greater than those of the pure components. All

of the blend films exhibited one composition-dependent glass transition temperature, suggesting that partial miscibility between H-chitosan and PLA molecules may be possible in the bulk amorphous phase. The melting behavior of the as-cast blend films exhibited double endothermic peaks, with both of the peak values being slightly lower than those of the pure PLA and no significant dependency on the blend composition being observed. The apparent degree of crystallinity of the PLA component in the blend films was found to monotonically decrease with addition and increasing H-chitosan content. Lastly, both the tensile strength at break and the Young's modulus of the blend films were found to decrease from that of the pure PLA to that of the pure H-chitosan with increasing H-chitosan content.

6.6 ACKNOWLEDGMENTS

The authors wish to thank partial support from the Petroleum and Petrochemical Technology Consortium (through a governmental load from the Asian Development Bank) and from the Petroleum and Petrochemical College, Chulalongkorn University.

6.7 REFERENCES

[1] Roberts, G. A. F. *Chitin Chemistry*; Palgrave Macmillan: London, 1992.

[2] Ravi Kumar, M. N. V. *Reactive and Functional Polymers* 2000, 46, 1.

[3] Nishimura, S. I.; Kohgo, O.; Kurita, K. *Macromolecules* 1991, 24, 4745.

[4] Yalpani, M.; Hall, L. D. *Macromolecules* 1984, 17, 272.

[5] Hirano, S.; Ohe, Y.; Ono, H. *Carbohydrate Research* 1976, 47, 315.

[6] Moore, G. K.; Roberts, G. A. F. *International Journal of Biological Macromolecules* 1981, 3, 292.

[7] Zong, Z.; Kimura, Y.; Takahashi, M.; Yamane, H. *Polymer* 2000, 41, 899.

[8] Seo, Y.; Ohtake, H.; Unishi, T.; Iijima, T. *Journal of Applied Polymer Science* 1995, 58, 633.

[9] Hirano, S.; Usutani, A.; Yoshikawa, M.; Midorikawa, T. *Carbohydrate Polymers* 1998, 37, 311.

[10] Xu, D.; McCarthy, S. P.; Gross, R. A.; Kaplan, D. L. *Macromolecules* 1996, 29, 3436.

[11] Lee, K. Y.; Ha, W. S.; Park, W. H. *Biomaterials* 1995, 16, 1211.

[12] Hirano, S.; Noishiki, Y. *Journal of Biomedical Materials Research* 1985, 19, 413.

[13] Fambri, L.; Pegoretti, A; Fenner, R.; Incardona, S. D.; Migliaresi, C. *Polymer* 1997, 38, 79.

[14] Khang, G.; Rhee, J. M.; Jeong, J. K.; Lee, J. S.; Kim, M. S.; Cho, S. H.; Lee, H. B.; *Macromolecular Research* 2003, 11, 207.

[15] Bergsma, J. E.; Bos, R. R. M.; Rozema, F. R.; Jong, W. D.; Boering, G. *Journal of Materials Science – Materials In Medicine* 1996, 7, 1.

[16] Bergsma, J. E.; Rozema, F. R.; Bos, R. R. M.; Boering, G.; Brujin, W. C.; Pennings, A. J. *Biomaterials* 1995, 16, 267.

[17] Rafler, G.; Dahlmann, J.; Wiener, K. *Acta Polymerica* 1990, 41, 328.

[18] Cohn, D.; Younes, H. *Journal of Biomedical Materials Research* 1988, 22, 993.

[19] Liu, C.; Mather, P. T. *Journal of Applied Medical Polymers* 2002, 6, 47.

[20] Supaphol, P. *Journal of Applied Polymer Science* 2001, 82, 1083.

[21] Srimoaon, P; Dangseeyun, N.; Supaphol, P. *European Polymer Journal* 2004, 40, 599.

[22] Fischer, E. W.; Sterzel, H. J.; Wegner, G. *Kolloid-Zeitschrift and Zeitschrift fur Polymere* 1973, 251, 980.

[23] Kister, G.; Cassanas, G.; Vert, M. *Polymer* 1998, 39, 267.

6.8 CAPTION OF FIGURES

Figure 6.1 A synthesis route for perfect H-chitosan.

Figure 6.2 FT-IR spectra of pure H-chitosan, pure PLA, and H-chitosan/PLA blend films.

Figure 6.3 FT-IR spectra of H-chitosan, pure PLA, and H-chitosan/PLA blend films illustrating the crystalline region of PLA.

Figure 6.4 TGA curves for pure H-chitosan, pure PLA, and 50/50 w/w H-chitosan/PLA blend films. The heating rate used was $10°C \cdot min^{-1}$.

Figure 6.5 Second heating thermograms for pure H-chitosan, pure PLA, and H-chitosan/PLA blend films. The heating rate used was $10°C \cdot min^{-1}$.

Figure 6.6 Scanning electron micrographs for as-etched H-chitosan/PLA blend films having the weight-based H-chitosan/PLA compositions of a) 20/80, b) 40/60, c) 50/50, d) 50/50, e) 60/40, and f) 80/20, respectively.
Figures a-c were etched by cyclohexane, while figures d-f were etched by concentrated acetic acid solution.

Figure 6.7 WAXD patterns for pure H-chitosan, pure PLA, and H-chitosan/PLA blend films.

Figure 6.8 a) Tensile strength at break, b) percentage of elongation at break, and c) Young's modulus for pure H-chitosan, pure PLA, and H-chitosan/PLA blend films plotted as a function of H-chitosan content.

Table 6.1 Thermal decomposition temperature(s) of pure H-chitosan, pure PLA, and H-chitosan/PLA blend films

Blend composition (H-chitosan/PLA) (w/w)	1^{st} T_d (°C)	2^{nd} T_d (°C)
0/100	-	327 ± 2
20/80	-	336 ± 0
40/60	264 ± 0	316 ± 1
50/50	254 ± 1	312 ± 2
60/40	255 ± 3	313 ± 1
80/20	257 ± 2	309 ± 1
100/0	257 ± 0	327 ± 2

Table 6.2 Glass transition temperature, low-temperature melting peak, high-temperature melting peak, apparent enthalpy of fusion, and apparent degree of crystallinity of pure H-chitosan, pure PLA, and H-chitosan/PLA blend films

Blend composition (H-chitosan/PLA) (w/w)	T_g (°C)	T_{ml} (°C)	T_{mh} (°C)	ΔH_f ($J \cdot g^{-1}$)	χ_c (%)
0/100	50 ± 1	162 ± 1	170 ± 1	21.7 ± 0.2	23.3 ± 0.2
20/80	46 ± 1	158 ± 0	168 ± 0	9.6 ± 0.8	12.9 ± 4.3
40/60	43 ± 2	159 ± 1	168 ± 1	6.9 ± 0.8	12.4 ± 2.2
50/50	42 ± 1	159 ± 1	168 ± 2	3.7 ± 0.4	7.9 ± 0.9
60/40	42 ± 0	160 ± 0	169 ± 0	3.3 ± 0.9	8.9 ± 1.6
80/20	43 ± 2	-	168 ± 0	1.5 ± 0.7	8.2 ± 0.9
100/0	-	-	-	-	-

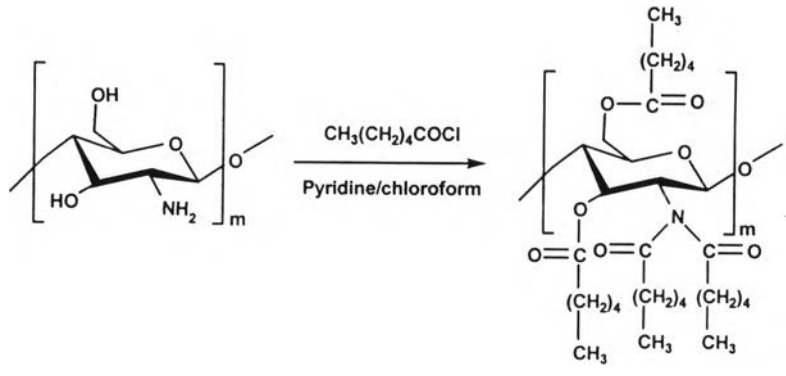
OH
HO
NH2
m
CH3(CH2)4COCl
Pyridine/chloroform
CH3
(CH2)4
O
C
O
N
(CH2)4
CH3

Figure 6.1

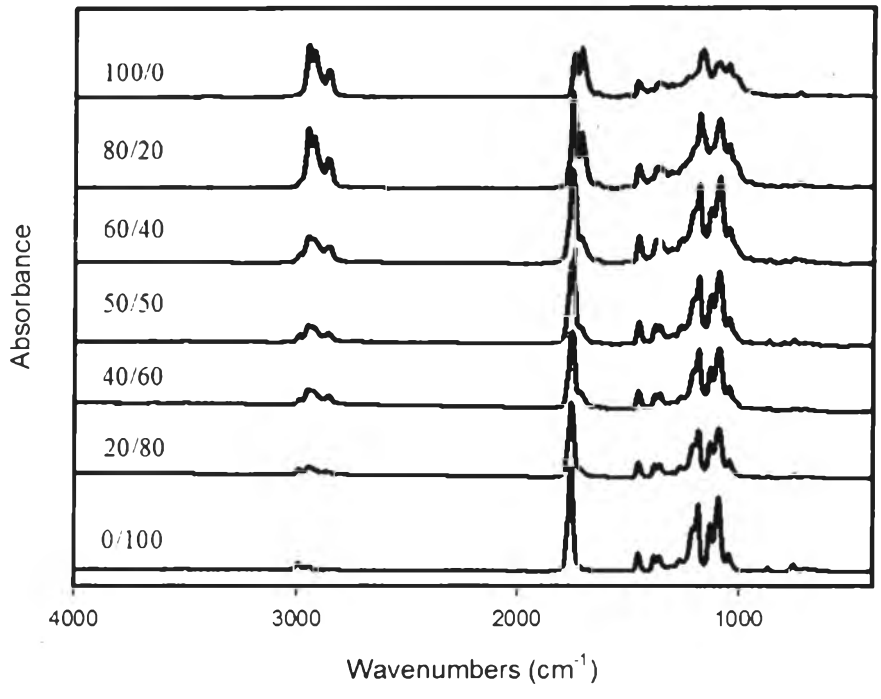
100/0
80/20
60/40
50/50
40/60
20/80
0/100
Absorbance
4000
3000
2000
1000
Wavenumbers (cm-1)

Figure 6.2

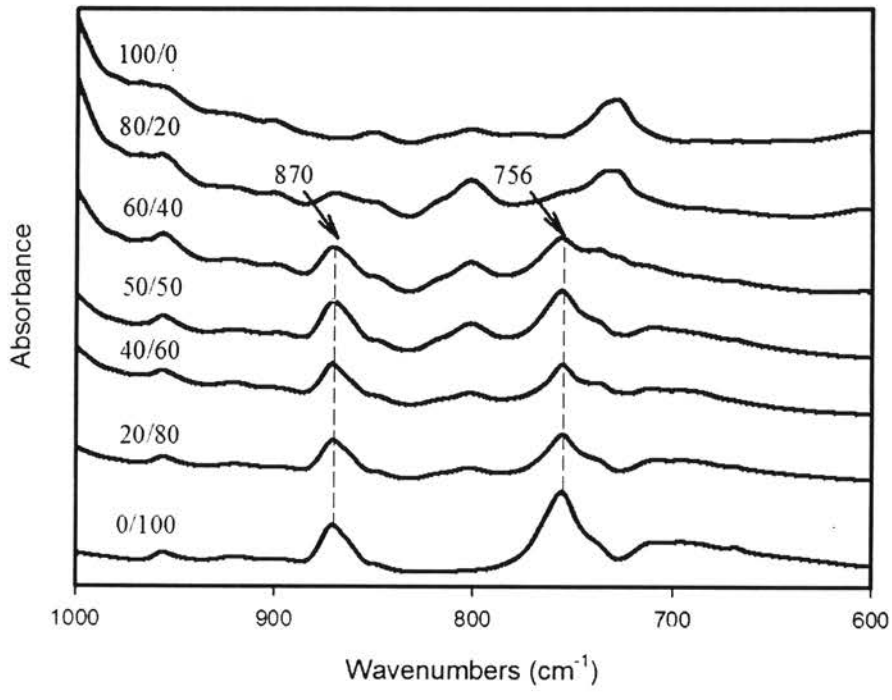
100/0
80/20
870
756
60/40
50/50
40/60
20/80
0/100
Absorbance
1000
900
800
700
600
Wavenumbers (cm-1)

Figure 6.3

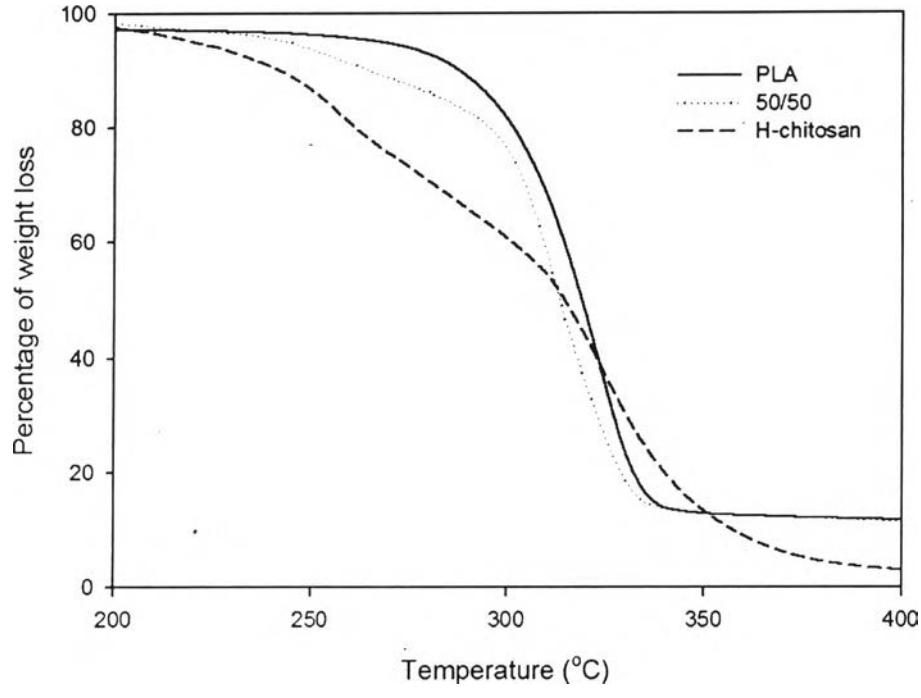
100
80
60
40
20
0
200
250
300
350
400
Percentage of weight loss
Temperature (°C)
PLA
50/50
H-chitosan

Figure 6.4

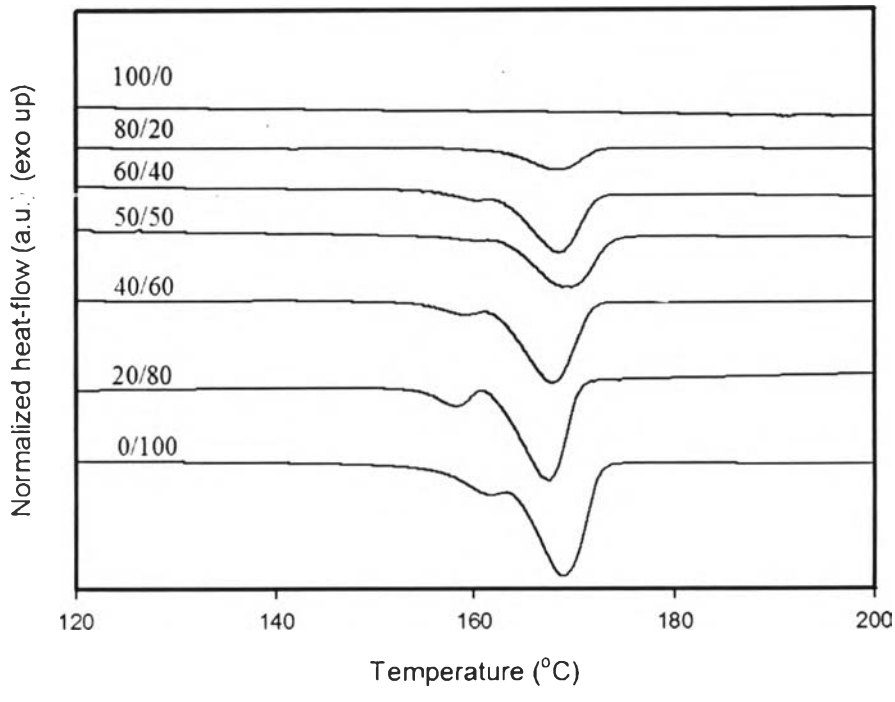
100/0
80/20
60/40
50/50
40/60
20/80
0/100
Normalized heat-flow (a.u.) (exo up)
120
140
160
180
200
Temperature (°C)

Figure 6.5

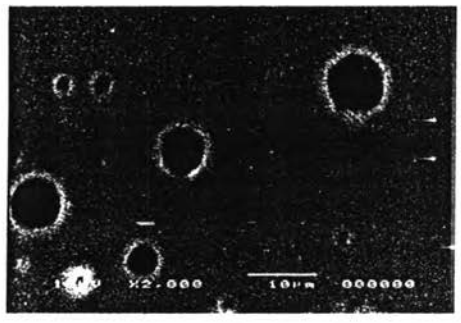

(a)

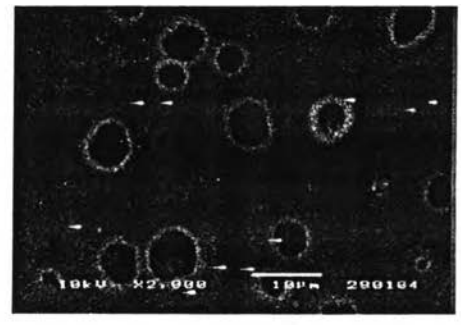

(b)

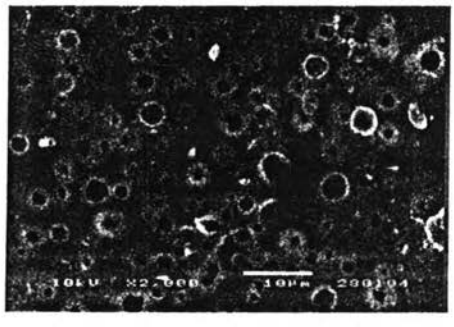

(c)

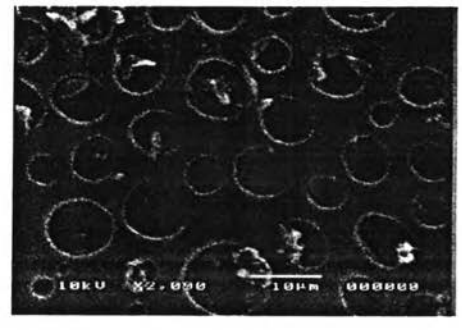

(d)

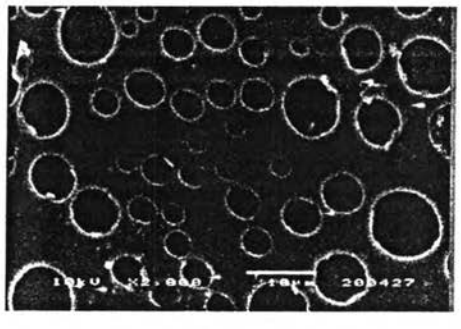

(e)

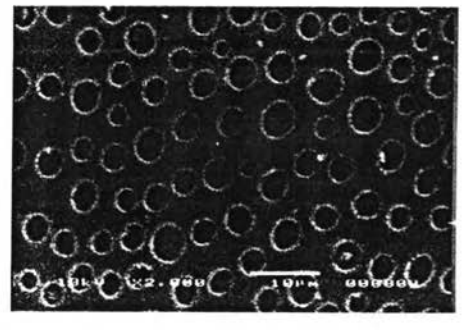

(f)

Figure 6.6

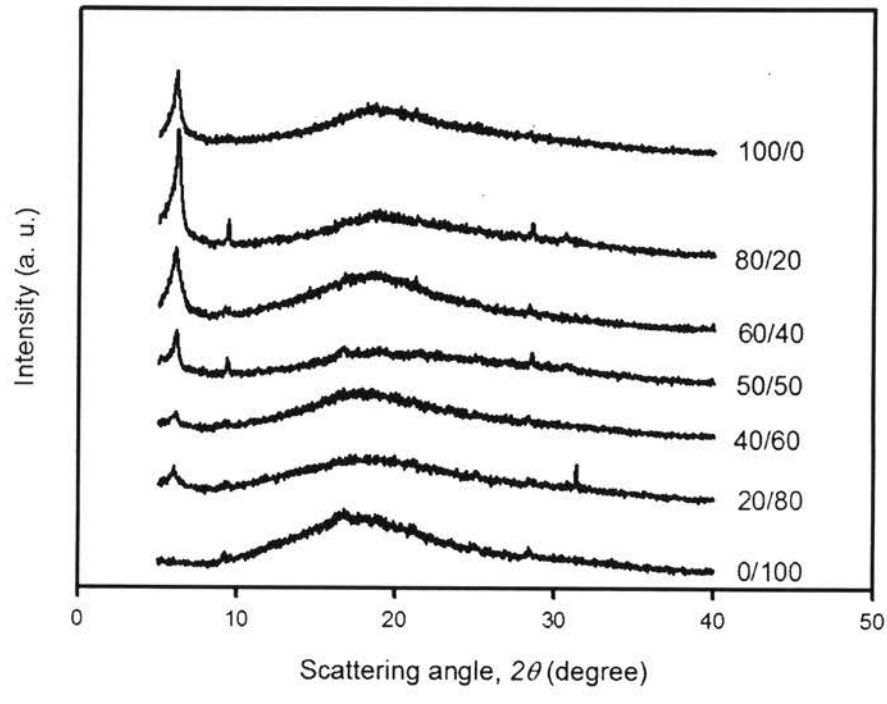
Intensity (a. u.)
100/0
80/20
60/40
50/50
40/60
20/80
0/100
0
10
20
30
40
50
Scattering angle, 2θ (degree)

Figure 6.7

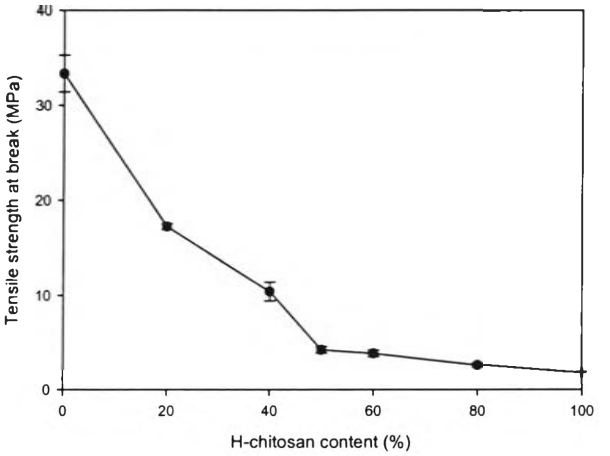

(a)

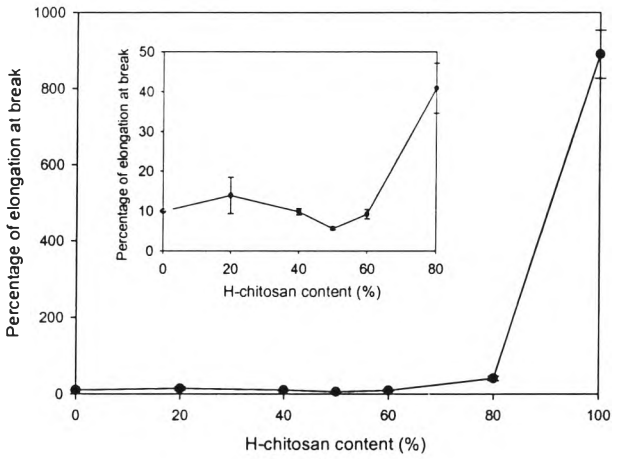

(b)

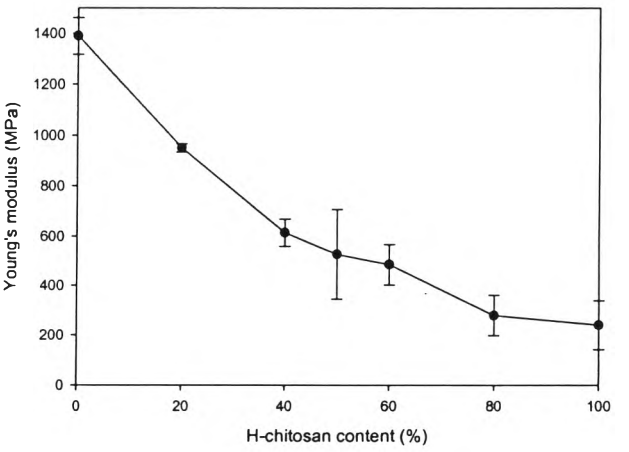

(c)

Figure 6.8